11

Plasma-Chemical Kinetics of Film Deposition in Argon-Methane and Argon-Acetylene Mixtures Under Atmospheric Pressure Conditions

Ramasamy Pothiraja, Nikita Bibinov and Peter Awakowicz
Institute for Electrical Engineering and Plasma Technology,
Ruhr-University Bochum,
Germany

1. Introduction

Understanding chemical kinetics of precursor dissociation and other follow-up plasma chemical reactions at atmospheric pressure plasma conditions is very important area of research for the development of plasma based film coating processes. It is very useful especially for coating on complex geometries like tubes, bottles, etc. Coating thin films on inner surface of tubes improves their functionality in many ways without changing the bulk properties. It improves the value of commercial tubes by improving their surface properties such as hydrophilicity, corrosion or permeation resistance and biocompatibility as in the following cases, 1. Depositing the fluorinated carbon on PVC tubes enhances the biocompatibility for the blood circulating tubes (Babukutty et al., 1999; Prat et al., 2000), 2. Silica coating on PTFE tube increases the wettability of the tube about 3 times (Yoshiki et al., 2006), 3. Carbon or titanium nitride film as protective coating on inner surface of a metallic tube improves its lifetime (Fujiyama, 2000; Hytry et al., 1994; Wang et al., 2008), 4. Deposition of silica on inner surface of PET tubes or bottles reduces the permeation of gases (Deilmann et al., 2008, 2009), 5. Titania coating on inner surface of glass tube improves its surface properties to be suitable for microfluidic devices (Yoshiki & Mitsui, 2008; Yoshiki & Saito, 2008), 6. Coating of nickel/alumina film on inner surface of silica tube and plasma treatment of resultant film increases the catalytic activity of this film for carbon nanofiber synthesis (Agiral et al., 2009). There are many ways film can be coated on various objects. Among those, "cold" plasma based film coating methods have many advantages compared to the conventional thermal film coating methods and spray coating methods. In plasma coating methods, electron will have high temperature (a few eV); however, atomic and molecular species will have low temperature (<0.1 eV). Because of this, precursors can be dissociated at relatively low gas temperature through electron impact. Hence, the plasma technology can be used for film coating on thermo-labile plastic materials. The advantage of using atmospheric pressure plasma source for film deposition is that it does not require vacuum system and hence it is economically favourable method of film coating. Especially for thin film deposition on inner surfaces of tubes, atmospheric pressure plasma is more suitable than low pressure plasma. In this regard, several research groups have developed this process and coated various films like SiO_2 and TiO_2 on inner surface of various metal, quartz, PET and PTFE tubes (Agiral et al., 2009; Babukutty et al., 1999; Deilmann et al., 2008,

2009; Foest et al., 2007; Fujiyama, 2000; Hytry et al., 1993, 1994; Prat et al., 2000; Wang et al., 2008; Yoshiki et al., 2006; Yoshiki & Mitsui, 2008; Yoshiki & Saito, 2008). Mostly microwave or RF driven ICP, CCP and jet based microplasma or magnetron plasma sources were used for their studies. Generally, in several methods used for coating films on inner surface of tubes, precursors are decomposed in the confined electrode region where the plasma is active, chemically active species are transported inside a tube and film coating is carried out by gas flow. In this case, because of polymerization and recombination reactions during the transport process, the nature of chemically active species (constituent of polymer film) is different at different places along the axis of the tube. This phenomenon could reduce the film uniformity along the axis of the tube. Our strategy for film coating on inner surface of tubes is to generate long plasma filaments inside the tube in a gas containing a precursor as an admixture (Pothiraja et al., 2010). The plasma filament, which will be thinner than the diameter of the tube to be coated, will be active for long distance in the region of film coating. This plasma filament can ionize and/or dissociate precursor molecules. Using this method, chemically active species can be generated everywhere along the axis of the tube within close vicinity of inner surface of the tube. In this way, differences in the nature of depositing chemically active species at different places along the axis of the tube can be reduced and films with better uniformity can be deposited. In addition to this, film deposition is supported by ion fluxes, which results the formation of high quality film.

In this regard, pulsed filamentary plasma source has been constructed, and long plasma filaments (longer than 100 mm) are generated inside the tube in the presence of methane or acetylene as a precursor. Using this, carbon based film is coated on inner surface of tubes and deposited film has been characterized using various surface analysis techniques. Understanding film properties on the basis of chemical kinetics of precursor dissociation, other gas phase and inter-phase reactions is very important. Hence chemical kinetics of these reactions is simulated. Since plasma parameters (electron density, electron velocity distribution function (EVDF)) play very important role in these reactions, they have been determined using emission spectroscopy, current-voltage measurement, microphotography and numerical simulation. In this chapter, we describe 1. Reaction schemes considered in our model for the determination of plasma parameters, 2. Influence of plasma parameters on chemical kinetics of precursor dissociation and other gas phase reactions involved in the film growth processes, and 3. Effect of plasma chemical reaction kinetics and nature of precursor on film properties and film growth rates.

2. Experiments and model

Configuration of plasma source used for film coating on inner surface of tubes is discussed below. Following this, methodology used for the determination of plasma parameters, rate constants and high probable plasma chemical reactions are discussed.

2.1 Experimental setup

Our plasma source consists of a cylindrical tungsten driven electrode with a diameter of 1.6 mm. One end of this electrode is sharpened (spike) to a cone angle of 30^{o}, while the other end of the electrode is connected to a high voltage generator (Redline Technologies G2000). The output voltage and the pulse frequency of this generator can be controlled and varied from 0-20 kV and from 4-500 kHz, respectively. Each high voltage pulse exhibits a sequential profile with damped oscillations. A tube made of quartz with the inner diameter

of 6 mm, is used in order to test the feasibility of film deposition as well as to characterize the plasma ignited in this setup. Tungsten driven electrode is placed coaxially inside this tube (figure 1). A copper tube (length, 10 mm) is used as a movable grounded electrode, which is placed coaxially on the outer surface of the quartz tube. For all the experiments reported in this chapter, the grounded electrode is fixed at 140 mm away from the spike of the driven electrode.

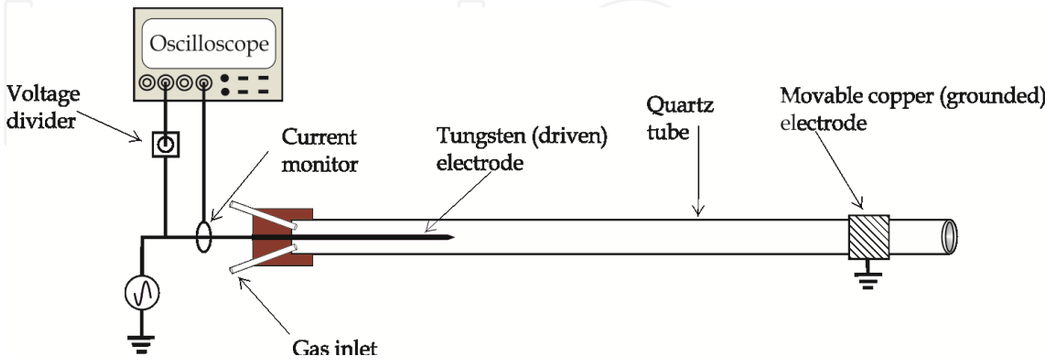

Fig. 1. Schematic view of experimental setup

We have used methane as well as acetylene as precursors. In both cases, we performed two sets of experiments. First set of experiments were carried out in argon and precursor mixture (Ar, 2400 sccm; CH_4, 3 sccm or C_2H_2, 2 sccm) to deposit carbon based film on inner surface of a quartz tube. Films deposited at this condition are characterized using various surface analysis techniques. Second set of experiments were carried out with argon, precursor and nitrogen gas mixture (Ar, 2400 sccm; CH_4 (or C_2H_2), 1 sccm; N_2, 2.5 sccm) for plasma characterization. Emissions of nitrogen molecules and nitrogen molecular ions are used for the determination of plasma parameters. Plasma parameters determined at this condition are considered to be the same as the plasma parameters during the film deposition process in the first set of experiments. The effect of absence of nitrogen on plasma parameters is balanced by increasing the precursor quantity. This fact (balancing of plasma parameters) is confirmed from the similar simulated EVDFs for both sets of experiments (with/without nitrogen). It is also confirmed by measuring argon emission spectra at various places along the axis of the tube in both cases. Argon emission intensities are very close to each other in both cases, and also have the similar trend along the axis of the tube.

Relatively and absolutely calibrated echelle spectrometer (ESA 3000) is used to obtain the emission spectra in a spectral range of 200 to 800 nm (Bibinov et al., 2007). Spectral resolution of the echelle spectrometer amounts to $\Delta\lambda$ = 0.015 nm at λ = 200 nm and $\Delta\lambda$ = 0.060 nm at λ = 800 nm. A Pearson current monitor (model, 6585; output, 1 V = 1 A) is used for plasma current measurement, which is mounted around a cable connecting the generator and the tungsten electrode. The output of the current monitor is connected to an oscilloscope (LeCroy *Wave Runner* 204MXi-A). Discharge duration is determined from the current profile. The actual voltage applied for plasma generation is measured by connecting the output of the generator to the oscilloscope through a capacitive voltage divider with the dividing factor of 2000. The pulse frequency of applied voltage is fixed as 22 kHz for all the experiments. For the plasma volume determination, a high speed sensitive CCD camera (PCO sensicam qe) is used. The spatial resolution of CCD camera amounts to 2 μm for an objective used with this camera.

2.2 Model

For diagnostics purposes, nitrogen is admixed with argon and precursor mixture. Plasma parameters are determined from the emission of neutral nitrogen molecules and molecular nitrogen ions. Our model used to obtain the information about gas temperature, plasma parameters and rate constants, from these emissions, are discussed below.

2.2.1 Plasma gas temperature

Gas temperature in active plasma volume is one of the important parameters, because of its influence on gas density in plasma as well as on the rate constants of chemical reactions. The rotational temperature of diatomic molecules is considered as the gas temperature, since the rotational and the translational degrees of freedom have equal temperatures because of very fast rotational relaxation at atmospheric pressure. For the determination of gas temperature, the rotational intensity distribution in the emission of neutral nitrogen molecule $N_2(C^3\Pi_u, \nu'=0 \rightarrow B^3\Pi_g, \nu''=0)$ (abbreviated as N_2(C–B, 0–0)) is used. The emission spectrum is measured perpendicular to the axis of the filament. Since the spectral resolution of our echelle spectrometer is not high enough to determine the intensities of the separate rotational lines in the emission spectrum of neutral nitrogen molecules, the rotational temperature is determined by a fitting procedure. For this purpose, we calculate the intensity distribution in the emission of N_2(C–B, 0–0) (λ = 337.1 nm) for different values of rotational temperature and spectral resolution used in the experiments, applying the program code developed for this purpose (Bibinov et al., 2001). By comparing the measured emission spectrum with the calculated spectra for various rotational temperatures, we determine the actual rotational temperature of nitrogen molecule with an inaccuracy of ±30 K.

When high concentration of the precursor is used, there is an overlap in the emission of N_2(C–B, 0–0) with the emission of NH radical at some places along the axis of the tube (filament). Hence, in this case, the rotational intensity distribution in the emission of CN radical, $CN(B^2\Sigma^+, \nu'=0 \rightarrow X^2\Sigma^+, \nu''=0)$ (CN(B–X, 0–0)) is used for the determination of gas temperature. In this case also, the rotational temperature is determined by the fitting procedure. In this regard, we simulate the intensity distribution in the emission of CN(B–X, 0–0) (λ = 388.3 nm) for different values of rotational temperature using the program LIFBASE (Luque & Crosley, 1999). The rotational temperature of CN radical is determined with an inaccuracy of ±30 K.

Under our experimental condition, molecular emissions N_2(C-B) and CN(B-X) are excited by electron impact as well as by collisions with argon metastable atoms (Nguyen & Sadeghi, 1983; Belikov et al., 1988). This effect can influence the rotational spectrum of nitrogen, and has been considered in the model. The angular momentum of heavy nucleus of diatomic molecules changes slightly by electron impact excitation. Therefore rotational distribution in molecular state excited by electron impact is equal to that in ground state, that means corresponds to the gas temperature. By excitation due to argon metastables, the rotational distributions in the excited states N_2(C) and CN(B) can be very different from rotational distributions at gas temperature. It can be approximately described by equilibrium distribution with temperature of about 2000K (Nguyen & Sadeghi, 1983; Belikov et al., 1988). Rotational distribution in measured emission spectrum is formed by initially excited distribution and competition of spontaneous emission, rotational relaxation and quenching

process by collisions with surrounding argon atoms. To study the influence of this factor on the reliability of measured gas temperature, we simulate the emission spectrum of N_2(C-B) for our experimental conditions with assumption that all "second positive system" in nitrogen emission spectrum is excited by collisions with argon metastables. To simulate the rotational relaxation, we use the rate constants determined in theoretical and experimental studies of rotational relaxation of nitrogen molecules in ground state by collisions with surrounding argon atoms (Belikov et al., 1988). The measured rotational distribution in N_2(C) excited during collisions with argon metastables (Nguyen & Sadeghi, 1983), and rate constant for quenching of N_2(C-B) emission in argon (Polak-Dingels & Djeu, 1983) are used for this simulation. After simulation of N_2(C-B) emission spectrum, we determine the rotational temperature using Boltzmann plot and estimate the deviation of determined value from the gas temperature assumed for our simulation. For our experimental conditions, this difference amounts to about 1% (e.g. 8 K at gas temperature of 800 K), which is much lower than the inaccuracy of ± 30 K of our fitting procedure.

The CN molecules are produced in $Ar/N_2/C_2H_2$ or $Ar/N_2/CH_4$ mixture through a multi-step reaction. The exact mechanism of formation and the rotational distribution of CN(B) state is not known in the literature. Therefore the rotational relaxation could not be simulated. However, because of the equal rotational temperatures of emission of N_2(C-B) and CN(B-X) determined at the same experimental conditions (see figure 2) and very fast relaxation of CN(B) in argon observed at low pressure conditions (Duewer et al., 1972), we conclude that CN(B)-molecule reach equilibrium rotational distribution before emitting of the photons. Hence, the influence of high rotational distribution after CN formation as well as excitation by collisions with argon metastables on the gas temperature determination by using CN molecular emission is also negligible.

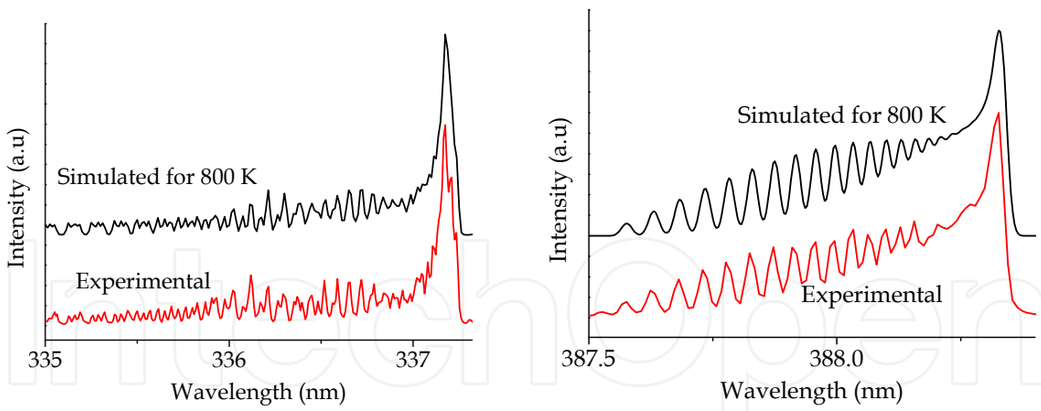

Fig. 2. Comparison of gas temperature determined by using the emission of N_2(C–B, 0–0) (left) and the emission of CN(B–X, 0–0) (right) from the same emission spectrum measured during the discharge. Simulated spectra are shifted for clarity.

2.2.2 Electron velocity distribution functions and rate constants

Electrons are the origin of most of the chemical reactions happening at atmospheric pressure plasma based processes; hence, their energy distribution plays an important role in plasma chemical reactions. The electron velocity distribution function (EVDF) in our system is determined on the basis of the emission of nitrogen molecule (equations 1-13). For this

purpose, absolute emission intensities of $N_2(C^3\Pi_u, \nu'=0 \rightarrow B^3\Pi_g, \nu''=0)$ (abbreviated as $I_{N_2(C\text{-}B)}$) and $N_2^+(B^2\Sigma_u^+, \nu'=0 \rightarrow X^2\Sigma_g^+, \nu''=0)$ ($I_{N_2^+(B-X)}$) are used. Since the threshold energy for the excitation of $N_2(X)$ to $N_2^+(B)$ by electron impact is different from the same for $N_2(X)$ to $N_2(C)$, the relative intensity of $I_{N_2^+(B-X)}$ with respect to the intensity of $I_{N_2(C-B)}$ is depending on the EVDF. On this basis, EVDF is determined using measured $I_{N_2^+(B-X)}$ / $I_{N_2(C-B)}$. For this purpose, we considered the following plasma chemical reactions (equations 1-9) for the determination of intensity of nitrogen emission (equations 10, 11).

$$N_2 + e \xrightarrow{k_{N_2^+(B)}} N_2^+(B) + 2e \quad (1)$$

$$N_2 + e \xrightarrow{k_{N_2(C)}} N_2(C) + e \quad (2)$$

$$N_2 + Ar_{met} \xrightarrow{k_{N_2(C)}^{Ar_{met}}} N_2(C) + Ar \quad (3)$$

$$\longrightarrow N_2(B) + Ar \quad (4)$$

$$Ar + e \xrightarrow{k_{Ar_{met}}} Ar_{met} + e \quad (5)$$

$$Ar_{met} + e \xrightarrow{k_{qAr_{met}}^{e}} Products \quad (6)$$

$$Ar_{met} + 2Ar \xrightarrow{k_{qAr_{met}}^{2Ar}} Products \quad (7)$$

$$Ar_{met} + N_2 \xrightarrow{k_{qAr_{met}}^{N_2}} Products \quad (8)$$

$$Ar_{met} + Prec \xrightarrow{k_{qAr_{met}}^{Prec}} Products \quad (9)$$

$$I_{N_2(C-B)} = (k_{N_2(C)} + K_{N_2(C)}^{Ar_{met}}) \cdot n_e \cdot [N_2] \cdot Q_{N_2(C)} \cdot g_f \cdot V_p \cdot t_f \quad (10)$$

$$\frac{I_{N_2^+(B-X)}}{I_{N_2(C-B)}} = \frac{Q_{N_2^+(B)}}{Q_{N_2(C)}} \cdot \frac{k_{N_2^+(B)}}{k_{N_2(C)} + K_{N_2(C)}^{Ar_{met}}} \quad (11)$$

where,

$$Q = \frac{A}{A + k_{qN_2}^{Ar} \cdot [Ar]} \quad (12)$$

$$K_{N_2(C)}^{Ar_{met}} = \frac{[Ar] \cdot k_{N_2(C)}^{Ar_{met}} \cdot k_{Ar_{met}} \cdot (B1) \cdot (B2)}{n_e \cdot k_{qAr_{met}}^{e} + [Ar]^2 \cdot k_{qAr_{met}}^{2Ar} + [N_2] \cdot k_{qAr_{met}}^{N_2} + [Prec] \cdot k_{qAr_{met}}^{Prec}} \quad (13)$$

$k_{N_2^+(B)}$ and $k_{N_2(C)}$ - electron impact excitation rate constants of nitrogen molecular emission, N_2^+(B-X) and N_2(C-B) respectively;

$k_{N_2(C)}^{Ar_{met}}$ - rate constant for the formation of N_2(C) by collision of N_2(X) with argon metastable (2.80×10^{-11} $cm^3 \cdot s^{-1}$) (Polak-Dingels & Djeu, 1983);

$k_{Ar_{met}}$ - electron impact excitation rate constant for argon metastable formation;

$k_{qN_2}^{Ar}$ - rate constant for the quenching of the corresponding excited states of nitrogen during collision with argon (for N_2(C) 8.00×10^{-13} $cm^3 \cdot s^{-1}$ (Polak-Dingels & Djeu, 1983); for N_2^+(B) 2.00×10^{-10} $cm^3 \cdot s^{-1}$ (Tellinghuisen et al., 1972));

$k_{qAr_{met}}^{e}$ (2.00×10^{-7} $cm^3 \cdot s^{-1}$ (Ivanov & Makasyuk, 1990)), $k_{qAr_{met}}^{2Ar}$ (1.20×10^{-32} $cm^6 \cdot s^{-1}$ (Kolts & Setser, 1978)), $k_{qAr_{met}}^{N_2}$ (3.50×10^{-11} $cm^3 \cdot s^{-1}$ (Kolts et al., 1977)) and $k_{qAr_{met}}^{Prec}$ (5.50×10^{-10} $cm^3 \cdot s^{-1}$ and 5.60×10^{-10} $cm^3 \cdot s^{-1}$ (Velazco et al., 1978)) - rate constants for quenching of argon metastable during collision with electron, argon, nitrogen and precursors (methane and acetylene), respectively;

A - Einstein coefficient for spontaneous emission (2.38×10^7 s^{-1} for N_2(C-B) (Pancheshnyi et al., 2000); 1.52×10^7 s^{-1} for N_2^+(B-X) (Dilecce et al., 2010));

B1 - branching factor for (3) (value = 0.787) (Zhiglinski, 1994);

B2 - branching factor for N_2(C-B, 0-0) transition by emission from N_2(C,0) (value = 0.5) (Laux & Kruger, 1992);

n_e - electron density (cm^{-3});

[*Ar*] - density of argon (cm^{-3});

[N_2] - density of nitrogen (cm^{-3});

[*Prec*] - density of methane or acetylene (cm^{-3});

V_p – observed volume of plasma (cm^3);

g_f - geometrical factor relating the part of photons reaching the entrance hole of the optical fiber in the spectrometer;

t_f - value of fraction of time, in which plasma is active.

The equations (10-13) are derived on the basis that the population of N_2^+(B) from the ground state ion N_2^+(X) is negligible compared to the one from N_2(X). This is because the concentration of N_2^+(X) is negligible compared to the concentration of N_2(X) in the cases we studied. For the generation of N_2(C), only direct electron impact excitation from the ground state of nitrogen molecule N_2(X) and the excitation during collision with argon metastable are considered (Kolts et al., 1977; Sadeghi et al., 1981, 1989; Touzeau & Pagnon, 1978). Other possible mechanism of generation of N_2(C) by 'pooling' reactions of two metastables N_2(A) (Herron, 1999) is negligible because of relatively low density of metastables N_2(A). Quenching of N_2(C) and N_2^+(B) by argon is considered (Polak-Dingels & Djeu, 1983; Tellinghuisen et al., 1972; Touzeau & Pagnon, 1978). However, quenching of N_2(C) and N_2^+(B) by nitrogen and precursor is neglected because of low concentration of these admixtures (Legrand et al., 2001).

For the calculation of rate constants $k_{N_2^+(B)}$ and $k_{N_2(C)}$ for a particular EVDF under our experimental conditions, the following methodology is used.

The EVDF is simulated for our experimental conditions (gas composition, gas temperature, pressure, etc.) by numerical solution of the Boltzmann equation and varied electric field

applying the program code "EEDF" developed by Napartovich et al (Stefanovic et al., 2001). In this simulation, "local" approximation is applied, which is valid for atmospheric pressure. This EVDF is normalized to fulfill the equation (14):

$$4\pi\sqrt{2}\int_0^\infty f_v(E)\cdot\sqrt{E}\mathrm{d}E = 1 \tag{14}$$

By using this normalized EVDF and the known collisional cross section σ_{exc} (cm^2) for electron impact excitation of nitrogen emission (Itikawa, 2006), we calculate the rate constants k ($cm^3 \cdot s^{-1}$) for electron impact excitation of N_2(C-B, 0-0) and N_2^+(B-X, 0-0) emissions by using the equation (15):

$$k = 4\pi\sqrt{2}\int_0^\infty f_v(E)\cdot\sqrt{\frac{2C}{m_e}}\cdot E\cdot\sigma_{exc}(E)\mathrm{d}E, \tag{15}$$

where m_e is the mass of electron (g), E is the kinetic energy of electrons (eV) and $C = 1.602 \times 10^{-12}$ erg·eV^{-1}.

From these calculated rate constants and the quenching factors (Q in equation 12), values of ratio of intensities of nitrogen emissions (using equation 11) are calculated for various EVDFs. By comparing the calculated values of ratio of emission intensities with measured one, the actual EVDF and its corresponding reduced electric field are determined.

2.2.3 Electron density

Electron density (n_e in cm^{-3}) is determined by using the equation (16), from the measured absolute intensity of N_2(C-B, 0-0) emission ($I_{N_2(C\text{-}B)}$, phot·s^{-1}), the electron impact excitation rate constant for N_2(C-B, 0-0) emission ($k_{N_2(C)}$), contribution of argon metastable for the formation of N_2(C) ($K_{N_2(C)}^{Ar_{met}}$), density of nitrogen ([N_2]), contribution of the quenching of N_2(C) by Ar ($Q_{N_2(C)}$), the geometrical factor for the fraction of photons produced in plasma volume reaching the optical fiber (g_f), the plasma volume (V_p in cm^3), and value of fraction of time in which plasma is active (t_f).

$$n_e = \frac{I_{N_2(C-B)}}{(k_{N_2(C)} + K_{N_2(C)}^{Ar_{met}})\cdot[N_2]\cdot Q_{N_2(C)}\cdot g_f\cdot V_p\cdot t_f} \tag{16}$$

All measurements with our emission spectrometer are space and time averaged. However, plasma parameters during the discharge are spatially and temporally non-uniform (Veldhuizen et al., 2009). In order to find out the influence of this non-uniformity of the plasma parameters on the reliability of measurements obtained using our spectrometer, we have simulated the total emission spectrum of two plasma regions of equal volume observed simultaneously by our spectrometer. Very different plasma conditions are assumed for these two regions. The composition of gas mixture corresponding to the methane system is used for the simulations. By using the total emission spectrum of nitrogen simulated for these two regions with different plasma parameters, the average plasma parameters are calculated for our optical emission spectroscopic (OES) diagnostics.

By using these averaged plasma parameters, the rate of methane dissociation is calculated. This value is compared with the value of the rate of methane dissociation calculated for these two regions.

For this purpose, the reduced electric field of 300 Td is assumed for the first region while 3000 Td for the second region. Electron density values are assumed as 4.62 $x10^{11}$ and 5.00 $x10^{11}$ (in cm^{-3}) for the first and the second regions, respectively. In these plasma conditions, the intensity of N_2(C-B, 0-0), which is used for electron density determination, is equal in both regions. On this basis, we have calculated total intensities of emission of nitrogen for the combination of these two regions, in the way our spectrometer would have observed. From these calculated values of intensities, the averaged values of electric field and electron density are calculated as 1800 Td and 3.91 $x10^{11}$ cm^{-3}, respectively. The ultimate aim for determination of the plasma parameters is to obtain the dissociation rate of precursor molecule. Hence, by using these averaged values of electron density and the reduced electric field, the rate of methane dissociation is calculated for this combined region. In a similar way, the dissociation rate of methane is calculated for these two regions separately on the basis of the emission spectra simulated for a spatially resolved measurement. The sum of these two values obtained for the spatially resolved measurement, is compared with the value of methane dissociation rate for the combined region calculated using the averaged plasma parameters for the spatially averaged measurement. In this case, there is less than 4% deviation in the rate of methane dissociation in using averaged plasma parameters.

We did similar calculation by assuming very different electron density values for these two regions, as 7.96 $x10^{13}$ cm^{-3} and 5.00 $x10^{11}$ cm^{-3} for the first (E/N, 300 Td) and the second (E/N, 3000 Td) regions, respectively. For these values of electron density and the electric field, the intensity of N_2^+(B-X, 0-0) for these two regions is equal. In this case, there is 8% deviation in the value of rate of methane dissociation by using spatially averaged plasma parameters.

The low time resolution in OES diagnostics causes an error in electron density determination because of the error in the time factor. The inverse of the same time factor is used for determination of the rate of hydrocarbon dissociation from electron density. Hence, the error in the time factor during electron density determination will be canceled during determination of the rate of methane dissociation. Hence, despite the possible deviation of the averaged plasma parameters determined using our OES diagnostics, from the real spatial and temporal distribution of plasma parameters (EVDF and electron density), the dissociation rate of hydrocarbon molecules obtained using the averaged plasma parameters is reliable.

2.2.4 Temporal and spatial distribution of gas temperature as well as fluxes of chemically active species

In order to determine the temporal and spatial distribution of gas temperature as well as fluxes of chemically active species from the plasma filament towards the surface of the tube, we numerically solve the equations for thermal conductivity (17) and diffusion (18) for a cylindrical symmetry (Bibinov et al., 2007; Rajasekaran et al., 2009):

$$\frac{\partial T}{\partial t} = \nabla \cdot (\alpha(T) \nabla T) \tag{17}$$

$$\frac{\partial [M]}{\partial t} = \nabla \cdot (D(T) \nabla [M]) \tag{18}$$

where,

$$\alpha(T) = \frac{\lambda_{conduction}}{\rho \cdot C_p},$$

α(T) - thermal diffusivity,
$\lambda_{conduction}$- thermal conductivity,
ρ - density,
C_p - specific heat capacity,
D - diffusion coefficient.

3. Results and discussion

3.1 Plasma ignition and film deposition

The pulsed filamentary discharge is ignited (Pothiraja et al., 2010, 2011) in the mixture of argon and methane or acetylene precursor (figure 3). This discharge is similar to a positive streamer discharge in argon (Veldhuizen et al., 2002). This long filament of plasma generated along the axis of the tube during this discharge has a diameter of about 200 μm.

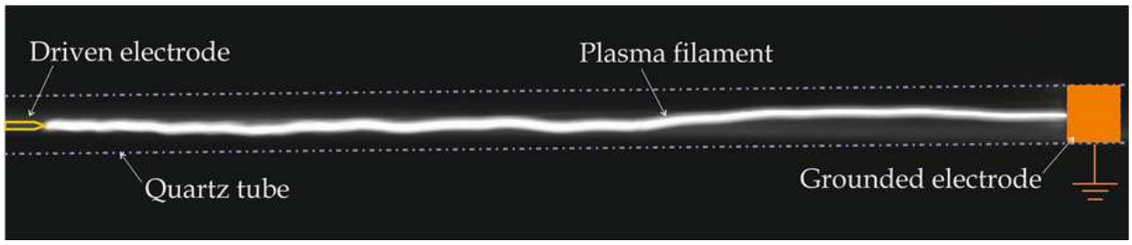

Fig. 3. Plasma filament ignited inside the tube in argon with precursor admixture.

The duration of the positive discharge is 160 ns (figure 4). During plasma operation, the profile and the position of filaments in the tube change with the frequency of several Hz. Because of this fact (profile and position of filaments are stationary for about 100 ms) and the pulse frequency is 22 kHz, about 2000 filaments in series have the same profile and position.

Emission spectra measured using echelle spectrometer for the discharge ignited in Ar/C_2H_2 as well as in Ar/CH_4 mixtures at different regions along the axis of tube indicates similar pattern. Measured spectra show characteristic emissions for the active species like C, C_2, CH, etc.; which indicates the dissociation of precursors, and participation of hydrocarbon radicals in film deposition (figure 5).

Films deposited at this condition are characterized using various surface analysis techniques. FTIR-ATR, XRD, SEM, LSM, Raman spectral and XPS analyses give the conclusion that when methane is used as a precursor, deposited film is amorphous

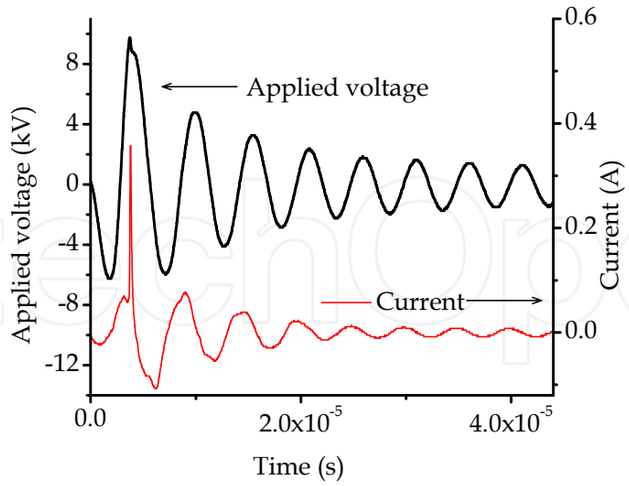

Fig. 4. Current-voltage profile during the positive filamentary discharge inside the tube

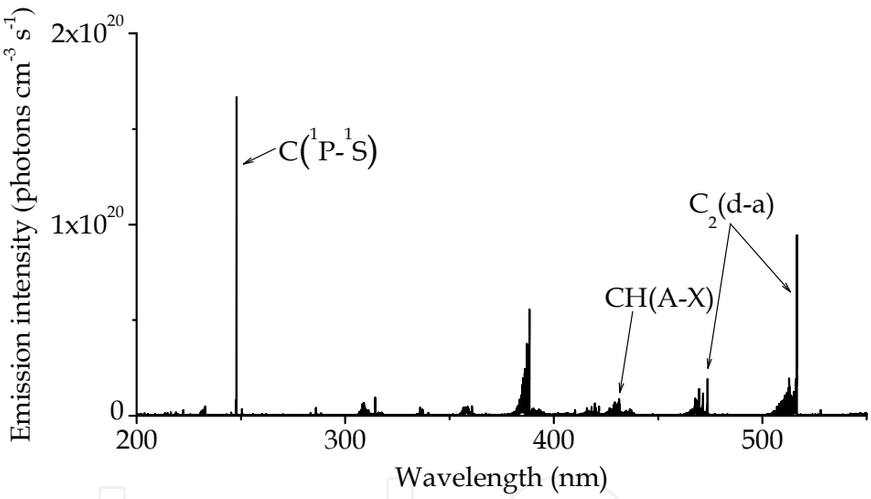

Fig. 5. Emission spectrum measured using echelle spectrometer for the discharge ignited in Ar/CH_4 mixture at the middle region in between the electrodes. Discharge in Ar/C_2H_2 mixture also shows similar emission spectrum

composed of non-hydrogenated sp^2 carbon and hydrogenated sp^3 carbon with traces of O and N (see figure 6, 7) (Murugavel & Pothiraja, 2003; Murugavel et al., 2007). UV-Vis absorption spectra of the film deposited on inner surface of the tube also confirm the presence of doubly bonded sp^2 carbon, which are shortly conjugated. When acetylene is used as a precursor, deposited film contains sp^1 carbon in addition to sp^2 and sp^3 hybridized carbon. Presence of sp^1 carbon in the film reduces the hardness of film, because of its linear structure which cannot form two dimensional or three dimensional structural networks. However, when acetylene is used as precursor, thickness of the film deposited on inner surface of the tubes, between the electrodes is more uniform than the same when methane is used as a precursor (figure 8).

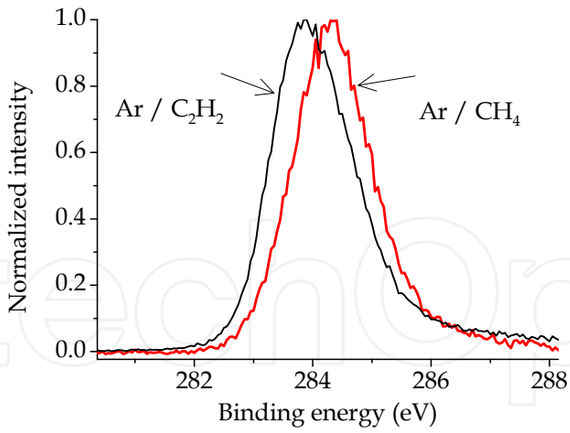

Fig. 6. XPS of carbon of the films deposited in filamentary discharges in Ar/C_2H_2 and Ar/CH_4 mixtures at middle region in between electrodes.

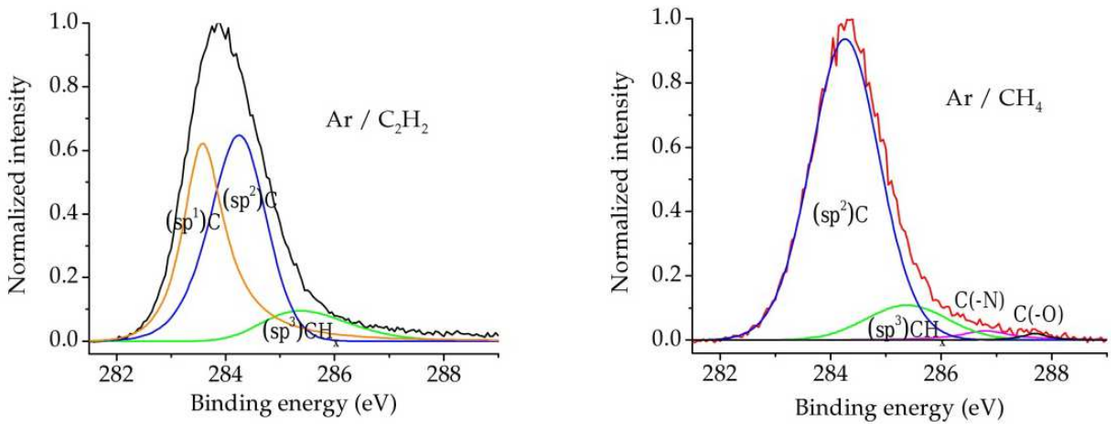

Fig. 7. XPS of carbon of the films deposited in filamentary discharge in Ar/C_2H_2 (left) and Ar/CH_4 (right) mixtures.

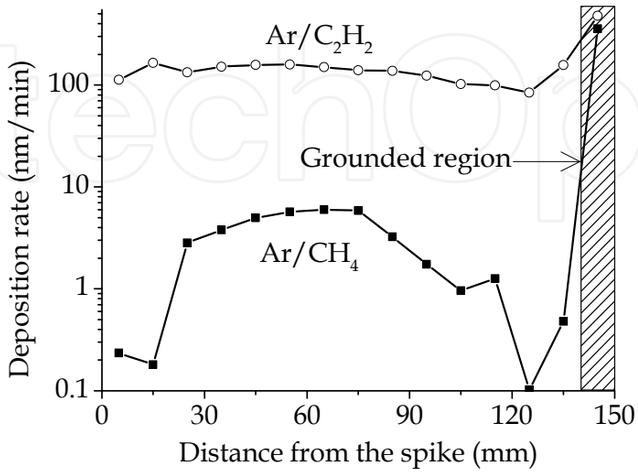

Fig. 8. Deposition rate of carbon based film inside of quartz tube by filamentary discharge in Ar/C_2H_2 and Ar/CH_4 mixtures.

Cross sectional images of the film deposited on quartz tube are obtained using LSM and SEM. From these images, film thickness is determined at 65 mm away from the spike (Pothiraja et al., 2009a, 2009b). By keeping this as reference, film thickness at various places along the axis of the tube is determined by measuring optical thickness of the film at these places on the basis of Beer-Lambert law in UV spectral range. The figure 8 shows growth rate at various places along the axis of the tube for the films deposited in Ar/C_2H_2 and Ar/CH_4 mixtures. For these experiments, similar quantities of methane as well as acetylene are used as precursor. As the figure 8 indicates, film growth rate in the grounded region is similar in both cases, and it is higher compared to the growth rate between the electrodes. When acetylene is used as a precursor, film growth rate between electrodes is about 30 times higher than the case where methane is used as precursor. It clearly indicates that plasma chemical reactions responsible for film growth process between the electrodes are different in these two cases. However, both precursor systems show similar film growth rates in the grounded region, and it is much higher than the film growth rate between the electrodes. This difference is very dominant methane system.

In order to understand these differences in the nature of the film, growth rate and thickness profile, we characterize plasma conditions (gas temperature in plasma filament, electron density, EVDF, etc.) in both cases. Using determined plasma parameters, we calculate production rates of atoms and excited molecules, simulated fluxes of excited chemical species to the inner surface of the tube, and simulated the chemical kinetics. We correlate the differences in the chemical kinetics on the differences in the film properties. OES, microphotography, current-voltage measurements and numerical simulations are used for the characterization of plasma conditions. Since the chemical kinetics depends on plasma conditions, plasma conditions and their differences between methane as well as acetylene cases are discussed first. Following this, differences in chemical kinetics will be discussed.

3.2 Gas temperature and tube temperature

The gas temperature determined in the plasma filament with both precursors at various places along the axis of the tube is shown in figure 9.

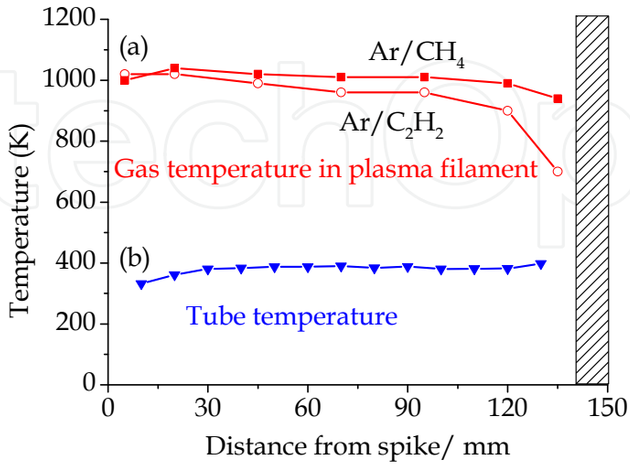

Fig. 9. Gas temperature in the plasma filament obtained using CN (B-X, 0-0) and N_2(C-B, 0-0) emissions (a), and tube temperature (b) along the axis of the tube during the pulsed filamentary discharge (Ar, 99.85%; N_2, 0.11%; CH_4 or C_2H_4, 0.04%; total gas flow rate, 2400 sccm)

The gas temperature in the plasma filament is about 1000 K. Although it is high (figure 9), duration of the discharge pulses is short: 160 ns (pulse frequency, 22 kHz). Therefore, the actual (stationary) temperature of tube will be much lower than the gas temperature in the plasma filament. The actual temperature of the tube during the discharge is measured using a thermocouple. It shows that tube temperature is less (about 330 K) close to the spike and it reaches about 400 K close to the grounded electrode (figure 9). Gas flow could be one of the reasons for this trend in tube temperature, since the gas mixture at room temperature is entering the spike region and relatively hot (or warm) gas mixture is entering the region close to the grounded electrode. With these data, equation for thermal conductivity is numerically solved to simulate the gas temperature in afterglow phase with temporal and spatial resolution. The results of this simulation presented in figure 10 show that the steady state conditions in the tube will be reached after 500 pulses. It is to be noted that, as mentioned before, about 2000 filaments in series have the same profile and position.

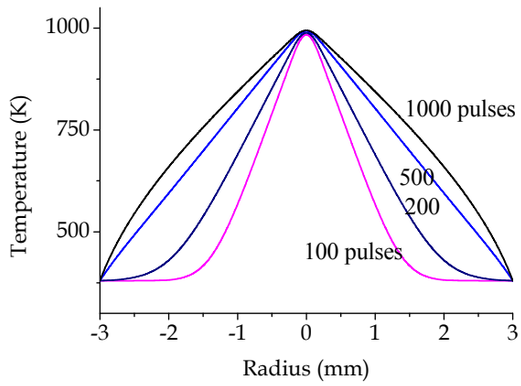

Fig. 10. Spatial distribution (in the radial direction) of the gas temperature from the plasma filament towards the surface of the tube. The filament diameter, 200 μm, is used for the simulations on the basis of micro-photographic images of the filaments

3.3 Plasma parameters

The reduced electric fields determined at different places along the axis of the tube during the discharge are shown in figure 11. It reveals that the reduced electric field has the same trend along the axis of tube, when methane is replaced with acetylene. However it reduces the magnitude of field to about 500 Td (figure 11). Reason for this trend in E/N along the axis of the tube is not clear now.

This change in E/N as methane is replaced with acetylene strongly influences the EVDF, as shown in figure 12. As a result of this, kinetics of electron impact plasma chemical reactions is not the same at different precursors as well as at different region along the axis of tubes.

As expected, difference in the reduced electric field also influences the electron density, when methane is replaced with acetylene. The electron density is almost constant in most part of the region in between the electrodes (figure 13). It is about 1.7×10^{12} cm^{-3} to 2.8×10^{12} cm^{-3}, when methane is used as precursor. However, when methane is replaced with acetylene, it is increased to about 8×10^{12} cm^{-3} to 3.8×10^{13} cm^{-3}. This increase in electron

density could be due to the additional mechanism of acetylene ionization during Penning ionization with argon metastables. These electron densities are about two orders of magnitude lower than the related streamer discharge known in the literature (Aleksandrov et al., 1999, 2001). This is because; we have determined the electron densities by assuming that plasma is active continuously between electrodes for all current pulse duration. In reality, the positive streamer head of length about a few mm with the diameter of about 200 μm is moving from one electrode to other electrode with the velocity of about 10^7 cm·s^{-1}. When this factor is considered, the electron densities determined through our method is well in agreement with the value reported in the literature for similar kind of plasma streamer. However, as discussed previously, this less temporally and spatially resolved plasma parameters will not affect considerably the determined overall plasma chemical kinetics parameters.

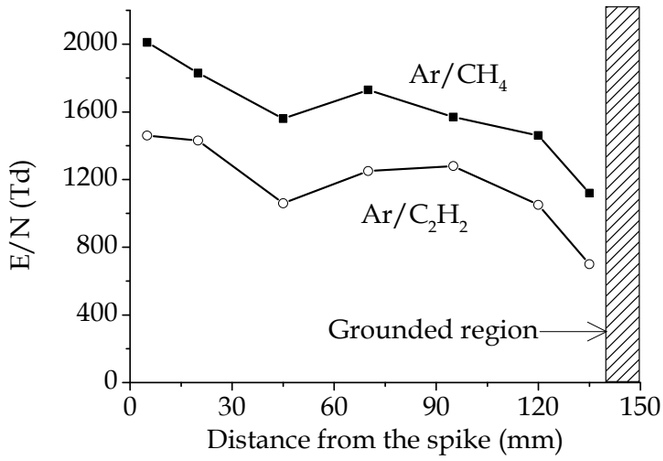

Fig. 11. Variation of the reduced electric field along the axis of the tube during the pulsed filamentary discharge

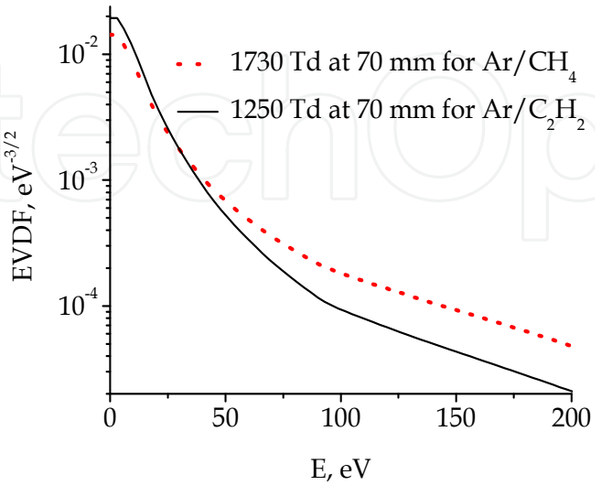

Fig. 12. The change in EVDF as methane admixture is replaced with acetylene in argon filamentary discharge.

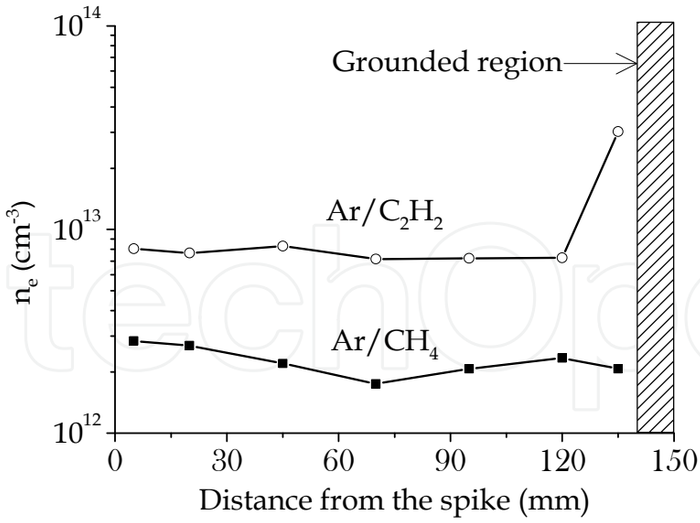

Fig. 13. Electron densities determined applying optical emission spectroscopy along the axis of tube for methane and acetylene plasma system.

3.4 Chemical kinetics

As mentioned previously, electron density and electron velocity distribution function play very important role in plasma (electron impact) chemical reactions. Therefore, the change in electron density and EVDF up on changing the precursor also changes the rate of electron impact excitation processes. The rate constants for electron impact acetylene and methane dissociation, argon ionization and argon metastables formation are determined (figure 14) using the equation (15), from the known values of cross-section for the corresponding process (Ballou et al., 1973; Belic et al., 2010; Garcıa & Manero, 1998; Khakoo et al., 2004) and the determined EVDF. Electron impact dissociation rate constant of precursor molecule is higher than the electron impact ionization rate constant of argon atom (figure 14). Despite this fact, because of the higher concentration of argon than precursor in the supplied gas mixture, electron impact argon ionization rate is much higher than the electron impact dissociation rate of precursor. Since the charge exchange reactions of argon ions with hydrocarbon molecules have big cross sections (Shul et al., 1987), mainly these reactions are

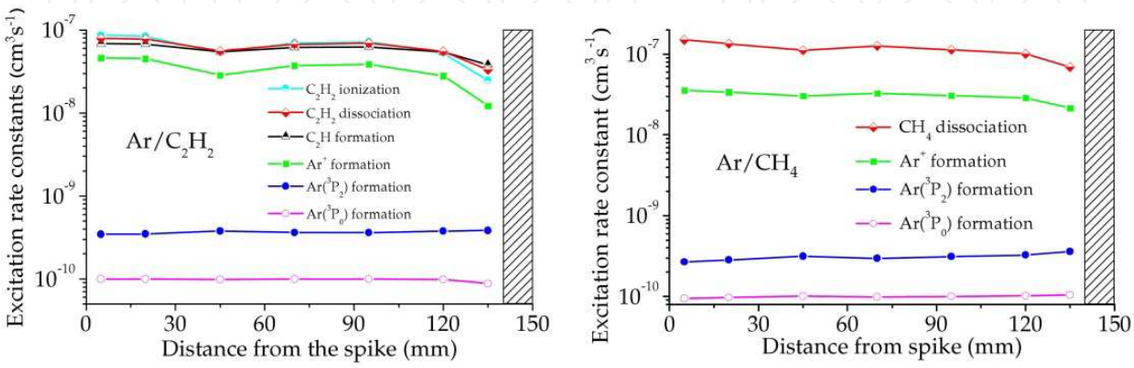

Fig. 14. Variation in the rate constants for electron impact acetylene dissociation, methane dissociation, argon ionization and argon metastables formation along the axis of the tube.

involved in the ionization and dissociative ionization of hydrocarbon species. Hence, argon ions play dominant role in the acetylene and methane ionization, dissociation and consequent film deposition processes. This is in contrast to the low pressure plasma chemical kinetics, where electron impact plays dominant role in acetylene and methane ionization, dissociation and consequent film deposition processes (Behringer, 1991; Moller, 1993; Pastol & Catherine, 1990).

Since the exact densities of various chemically active species and their diffusion coefficients are not known, methane diffusion in argon is simulated in order to have some hints about the diffusion of various chemically active species. Simulated results for methane diffusion in the figure 15 show that it takes about 10 to 20 ms for a chemically active species generated in the filament, which is approximately placed at the middle of the tube, to reach the tube surface. During this transport process, it may undergo several chemical reactions. Gas velocity is 1.4 $m \cdot s^{-1}$ for the gas flow rate of 2.4 slm. Hence, in the duration of 10 to 20 ms, neutral radicals will be moved to a distance of 1.5 to 3 cm along the axis of the tube.

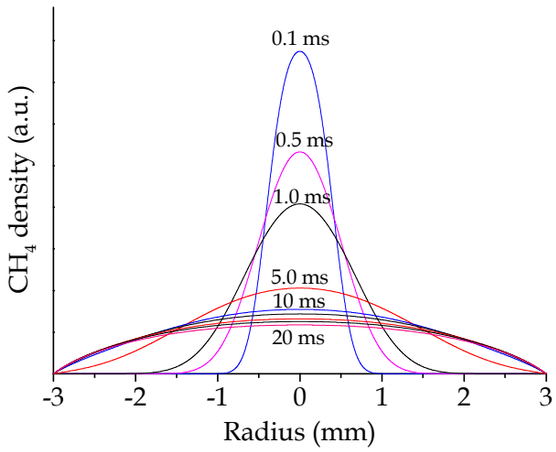

Fig. 15. Spatial distribution of chemically active species generated in the filament towards the surface of tube. Since several chemically active species are generated in the filament, CH_4 diffusion in Ar is simulated.

The next step is to find out differences in the plasma chemical reactions and their chemical kinetics between methane and acetylene cases. Since the same quantity of argon is used in both cases, a main difference on the basis of atomic composition of precursors is the following. In the case of methane, carbon and hydrogen ratio is 1:4, but it is 1:1 for acetylene. The difference in the quantity of hydrogen with respect to carbon is important for chemical kinetics. Because of small size of hydrogen atom, it has high mobility compared to all other elements in the plasma system. Second reason is that atomic hydrogen (hydrogen radical) is the most reactive part of neutral element in our plasma system. Hence a small change in the quantity of hydrogen especially with respect to carbon will have strong influence on the chemical kinetics of carbon based film growth process. The second important difference among the precursors is their reactivity. From chemical structure and bonding point of view, acetylene is more reactive than methane. This will have considerable influence on the

film coating process. Acetylene is the monomer of polymer, polyacetylene. It is more prone to undergo polymerization even without plasma in the presence of catalyst. Hence under plasma conditions, it can undergo polymerization reaction leading to high film growth rate. Other difference, which may affect the hardness of deposited film, is the hybridization of carbon in the precursor. Methane has sp^3 hybridized carbon, but acetylene has sp^1 hybridized carbon. It is well known that presence of sp^1 hybridized carbon will reduce the film hardness because of its linear structure, compared to a film composed of sp^2 and sp^3 carbon based materials. Also it is reported in the literature that methane is better precursor for hard film coating compared to acetylene (Fedosenko et al., 2001). By considering all above stated facts (nature of the precursor, plasma conditions and film properties), the most probable reactions among others are calculated using the equation (19), from the known values of densities of argon, methane and electron, as well as rate constants of various processes determined from the plasma parameters and known in the literature (Alman et al., 2000; Baulch et al., 1994; Denysenko et al., 2004; Pitts et al., 1982; Shiu & Biondi, 1978; Sieck & Lias, 1976; Tsang & Hampson, 1986),

$$P = ([M] \cdot k)^{-1} \tag{19}$$

where, P is the probability, $[M]$ is the density of reactant species (cm^{-3}), and k is the rate constant ($cm^3 \cdot s^{-1}$). The possible important chemical reactions for our experimental conditions are shown in the following scheme (figure 16 and 17). The high probable

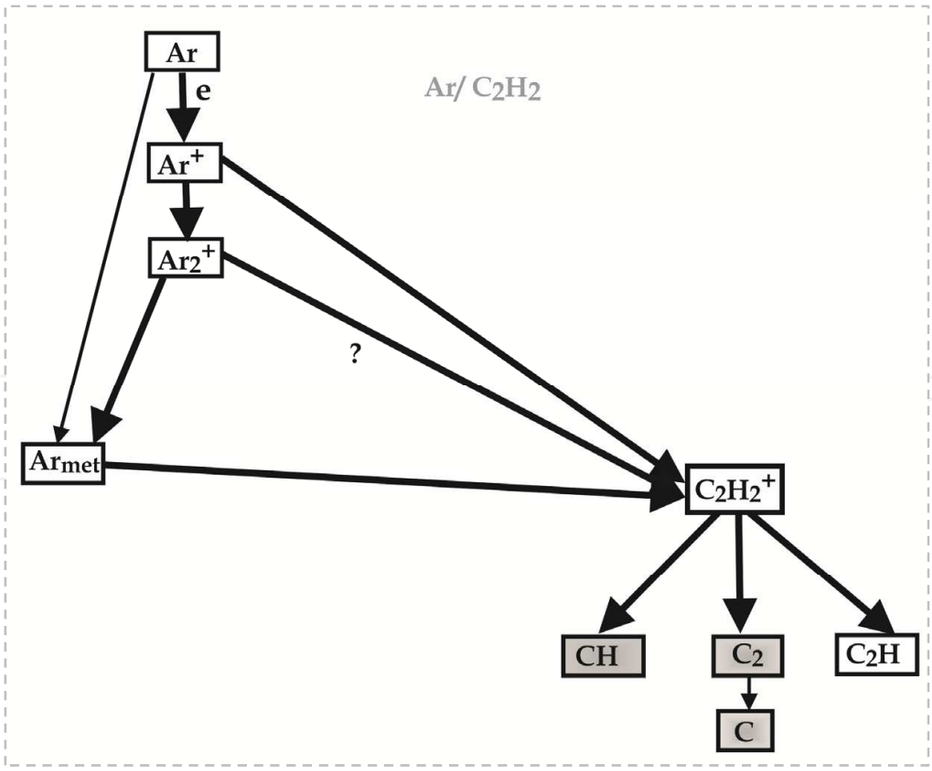

Fig. 16. Chemical reactions involved in the film growth process in filamentary discharge in Ar/C_2H_2 mixture. Thick arrow indicates high probable reaction.

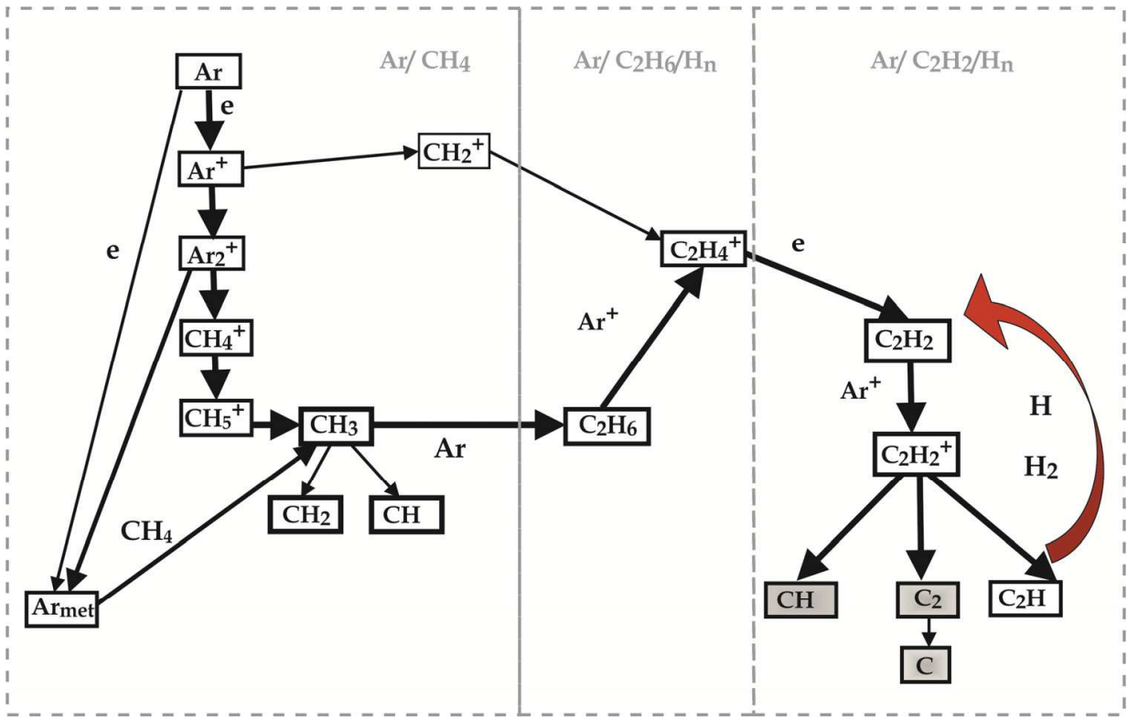

Fig. 17. Chemical reactions involved in the film growth process in filamentary discharge in Ar/CH_4 mixture. Thick arrow indicates high probable reaction. Species shown in gray boxes are observed through their characteristic emission.

reactions among others are shown in thick arrows in the scheme. Analyses of many possible reaction under our plasma conditions indicates that argon ion formation is more probable reaction than argon metastable formation reaction in both methane as well as acetylene cases. This is because of high reduced electric field in both plasma conditions. At atmospheric pressure conditions, Ar^+ ion produces molecular ion, Ar_2^+ through a three particles collision reaction. This is in contrast to the low pressure plasma, where the probability for three particles collision reactions is very low (Pastol & Catherine, 1990; Behringer, 1991; Moller, 1993; Bauer et al., 2005; Awakowicz et al., 2001; Horn et al., 1994). These argon ions undergo charge exchange reaction with precursors. In the case of acetylene, it produces $C_2H_2^+$. The charge exchange reaction of Ar^+ with C_2H_2 is known in the literature. Even though, similar charge exchange reaction of Ar_2^+ with C_2H_2 is not known, to our knowledge; under atmospheric pressure condition, it should have similar high probability.

In the case of methane, the charge exchange reactions produce CH_x^+. These ions through multistep reactions lead to the formation of C_2H_2. This process is very efficient, and it is known in the literature that methane can efficiently be converted in to acetylene in the spark discharge under atmospheric pressure plasma conditions (Leutner & Stokes, 1961; Yao et al., 2002). It indicates that even though it is started with methane, most of the methane will be converted in to acetylene under our plasma conditions. The acetylene produced in the

methane system has high probability to undergo charge exchange reactions with argon ions to produce $C_2H_2^+$, as in the case of acetylene system. This indicates that whether it is methane precursor or acetylene precursor, both lead to the formation of mainly $C_2H_2^+$.

In both systems, $C_2H_2^+$ produces reactive species, CH, C_2, C, C_2H, etc., for film deposition process. The presence of reactive species, CH, C_2 and C are observed experimentally (figure 5) through their characteristic emissions in the emission spectra measured for both cases. The reactive species C_2H has very high probability to undergo addition reaction with hydrogen to produce C_2H_2 (Farhat et al., 1993; Kovacs et al., 2010). In other words, presence of hydrogen in the plasma system regenerates acetylene, and hinders the film growth process. The hydrogen quantity with respect to carbon in methane system is four times higher than the same for acetylene. This indicates that film growth hindering reaction due to the presence of hydrogen in methane system is much higher than the same for acetylene system. Hence film growth rate in methane system is very less compared to the same for acetylene system. This fact is verified by externally adding hydrogen into the acetylene system. When three molar ratio of hydrogen molecule with respect to acetylene is added into acetylene system, the film growth rate is drastically reduced compared to the acetylene system without externally added hydrogen.

In the case of methane, at steady state conditions, precursor is fully ionized and dissociated in the tube at the distance of approximately 20 mm from the spike. However, the film deposition rate has sharp maxima under the grounded area, which is at 140 mm away from the spike. The film deposited in the area between the spike and the grounded electrode has different thickness at different places, but with similar properties and components. This film is dense and amorphous; has smooth surface and low content of hydrogen. We suppose that this film is deposited during ion fluxes (Bauer et al, 2005) on the wall after ambipolar diffusion and drift. In the frame of this assumption, we can explain different observed facts such as i) higher deposition rate in the region under grounded electrode because of higher drift velocity in comparison to the velocity of ambipolar diffusion, and ii) low deposition rate near the grounded area because of high axial component of electric field in this region. The hydrocarbon film deposited in the region beyond the grounded area is differed strongly from the film deposited before and under the grounded area. This film is soft, rough and low dense. This film may be deposited by flux of neutral hydrocarbon species which are produced by collisions of hydrocarbon ions with the surface of the tube under the grounded area. The kinetic energy of these ions is high enough for their partial dissociation. The neutral hydrocarbon species formed in this process flow with gas along the tube and deposit on the wall after diffusion. The mechanism of ions transport from the spike area to the grounded area is under investigation.

4. Conclusion

Chemical kinetics of methane and acetylene dissociation and other gas phase reactions are studied for film coating applications under atmospheric pressure plasma conditions. In order to determine the plasma parameters, OES, V-I measurement, micro-photography and numerical simulations are used. From the determined EVDF and n_e, electron impact plasma chemical reaction rates are determined. On the basis of rate of different possible reaction,

most probable reactions among others are calculated. From this information and atomic composition of precursors, film deposition rate and film properties are explained as follows, 1. Precursor molecules are ionized and dissociated mainly through charge exchange reaction of argon ions with precursor molecules. 2. Because of low quantity of hydrogen in acetylene, C_2H species dominates in the film deposition process, which facilitates the incorporation of sp^1 carbon in the film. 3. Presence of high quantity of hydrogen in methane facilitates the regeneration of acetylene from the reactive species C_2H; thus reducing film growth rate in methane plasma system in the region between electrodes. 4. Hydrocarbon ion fluxes plays dominant role in methane system, which is responsible for high growth rate in the grounded region. From this study, it can be concluded that atomic composition between carbon and hydrogen in the precursor plays very important role in carbon based film deposition process. Presence of atomic hydrogen in the plasma system improves the film hardness, but in the expense of film growth rate.

5. Acknowledgment

This work is supported by the 'Deutsche Forschungsgemeinschaft' (DFG) within the frame of the research group 'FOR1123 - Physics of Microplasmas'.

6. References

Ağıral, A.; Lefferts, L. & Gardeniers, J. G. E. (2009). Catalyst activation by microplasma for carbon nanofiber synthesis in a microreactor. *IEEE Trans. Plasma Sci.*, Vol.37, pp.985-992

Aleksandrov, N. L.; Bazelyan, E. M.; Gorunov, A. Y. & Kochetov, I. V. (1999). A non-thermal mechanism of spark breakdown in Ar. *J. Phys D: Appl. Phys.*, Vol.32, pp. 2636-2644

Aleksandrov, N. L.; Bazelyan, E. M. & Novitskii, G. A. (2001). The effect of small O_2 addition on the properties of a long positive streamer in Ar. *J. Phys D: Appl. Phys.*, Vol. 34, pp. 1374-1378

Alman, D. A.; Ruzic, D. N. & Brooks, J. N. (2000). A hydrocarbon reaction model for low temperature hydrogen plasmas and an application to the Joint European Torus. *Phys. Plasmas*, Vol. 7, pp. 1421-1432

Awakowicz, P.; Schwefel, R.; Scheubert, P. & Benstetter, G. (2001). Deposition of a-C:H films with an ECWR-reactor at 27 MHz: plasma diagnostics and film properties. *Surf. Coat. Technol.*, Vol. 142-144, pp. 342-347

Babukutty, Y.; Prat, R.; Endo, K.; Kogoma, M.; Okazaki, S. & Kodama, M. (1999). Poly(vinyl chloride) surface modification using tetrafluoroethylene in atmospheric pressure glow discharge. *Langmuir*, Vol. 15, pp. 7055-7062

Ballou, J. K.; Lin, C. C. & Fajen, F. E. (1973). Electron-impact excitation of the argon atom. *Phys. Rev.* A, Vol. 8, pp. 1797-1807

Bauer, M.; Schwarz-Selinger, T.; Jacob, W. & von Keudell, A. (2005). Growth precursors for *a*-C:H film deposition in pulsed inductively coupled methane plasma. *J. Appl. Phys.*, Vol. 98, p. 073302 (11pp)

Baulch, D. L.; Cobos, C. J.; Cox, R. A.; Frank, P.; Hayman, G.; Just, T.; Kerr, J. A.; Murrells, T.; Pilling, M. J.; Troe, J.; Walker, R. W. & Warnatz, J. (1994). Evaluated kinetic data for combustion modeling. Supplement I. *J. Phys. Chem. Ref. Data*, Vol. 23, pp. 847-848

Behringer, K. (1991). Diagnostics and modelling of ECRH microwave discharges. *Plasma Phys. Contr. Fusion*, Vol. 33, pp. 997-1028

Belic, D. S.; Lecointre, J. & Defrance, P. (2010). Electron impact multiple ionization of argon ions. *J. Phys. B: At. Mol. Opt. Phys.*, Vol. 43, p. 185203 (10pp)

Belikov, A. E.; Burshtein, A. I.; Dolgushev, S. V.; Storozhev, A. V.; Strekalov, M. L.; Sukhinin, G. I. & Sharafutdinov, R. G. (1989). Rate constants and rotational relaxation times for N_2 in argon. *Chem. Phys.*, Vol. 139, pp. 239-259

Bibinov, N. K.; Fateev, A. A. & Wiesemann, K. (2001). On the influence of metastable reactions on rotational temperatures in dielectric barrier discharges in He-N_2 mixtures. *J. Phys. D: Appl. Phys.*, Vol. 34, pp. 1819-1826

Bibinov, N.; Halfmann, H.; Awakowicz, P. & Wiesemann, K. (2007). Relative and absolute intensity calibrations of a modern broadband echelle spectrometer. *Meas. Sci. Technol.*, Vol. 18, pp. 1327-1337

Deilmann, M.; Theiß, S. & Awakowicz, P. (2008). Pulsed microwave plasma polymerization of silicon oxide films: Application of efficient permeation barriers on polyethylene terephthalate. *Surf. Coat. Technol.*, Vol. 202, pp. 1911-1917

Deilmann, M.; Halfmann, H.; Steves, S.; Bibinov, N. & Awakowicz, P. (2009). Silicon oxide permeation barrier coating and plasma sterilization of PET bottles and foils. *Plasma Process. Polym.*, Vol. 6, pp. S695-S699

Denysenko, I. B.; Xu, S.; Long, J. D.; Rutkevych, P. P.; Azarenkov, N. A. & Ostrikov, K. (2004). Inductively coupled Ar/CH_4/H_2 plasmas for low-temperature deposition of ordered carbon nanostructures. *J. Appl. Phys.*, Vol. 95, pp. 2713-2724

Dilecce, G.; Ambrico, P. F. & Benedictis, S. D. (2010). On the collision quenching of $N_2^+(B^2\Sigma_u^+, v=0)$ by N_2 and O_2 and its influence on the measurement of *E/N* by intensity ratio of nitrogen spectral bands. *J. Phys. D: Appl. Phys.*, Vol. 43, p. 195201 (7pp)

Duewer, W. H.; Coxon, J. A. & Setser, D. W. (1972). Collisional transition probabilities for rotational levels of $CN(B^2\Sigma^+)$. *J. Chem. Phys.*, Vol. 56, pp. 4355-4362

Farhat, S. K.; Morter, C. L. & Glass, G. P. (1993). Temperature dependence of the rate of reaction of C_2H with H_2. *J. Phys. Chem.*, Vol. 97, pp. 12789-12792

Fedosenko, G.; Schwabedissen, A.; Korzec, D. & Engemann, J. (2001). Diamond-like carbon film deposition by a 13.56 MHz hollow cathode RF-RF system using different precursor gases. *Surf. Coat. Technol.*, Vol. 142-144, pp. 693-697

Foest, R.; Kindel, E.; Lange, H.; Ohl, A.; Stieber, M. & Weltmann, K. –D. (2007). RF capillary jet – a tool for localized surface treatment. *Contrib. Plasma Phys.*, Vol. 47, pp. 119-128

Fujiyama, H. (2000). Inner coating of long-narrow tube by plasma sputtering. *Surf. Coat. Technol.*, Vol. 131, pp. 278-283

García, G. & Manero, F. (1998). Electron scattering by CH_4 molecules at intermediate energies (400–5000 eV). *Phys. Rev.* A, Vol. 57, pp. 1069-1073

Herron, J. T. (1999). Evaluated chemical kinetics data for reactions of N(^2D), N(^2P), and $N_2(A^3\Sigma_u^+)$ in the gas phase. *J. Phys. Chem. Ref. Data*, Vol. 28, pp. 1453-1483

Horn, A.; Schenk, A.; Biener, J.; Winter, B.; Lutterloh, C.; Wittmann, M. & Küppers, J. (1994). H atom impact induced chemical erosion reaction at C:H film surfaces. *Chem. Phys. Lett*., Vol. 231, pp. 193-198

Hytry, R.; Möller, W.; Wilhelm, R. & von Keudell, A. (1993). Moving-coil waveguide discharge for inner coating of metal tubes. *J. Vac. Sci. Technol.* A, Vol.11, pp. 2508-2517

Hytry, R.; Möller, W. & Wilhelm, R. (1994). Running waveguide discharge for inner coating of metal tubes. *Appl. Phys. Lett*., Vol. 64, pp. 3401-3403

Itikawa, Y. (2006). Cross section for electron collisions with nitrogen molecules. *J. Phys. Chem. Ref. Data*, Vol. 35, pp. 31-53

Ivanov, V. A. & Makasyuk, I. V. (1990). Destruction of Ar4s($^3P_2$) metastable atoms by slow electrons. *Opt. Spectrosc. (USSR)*, Vol. 69, pp. 308-310

Khakoo, M. A.; Vandeventer, P.; Childers, J. G.; Kanik, I.; Fontes, C. J.; Bartschat, K.; Zeman, V.; Madison, D. H.; Saxena, S.; Srivastava, R. & Stauffer, A. D. (2004). Electron impact excitation of the argon $3p^54s$ configuration: differential cross-sections and cross-section ratios. *J. Phys. B: At. Mol. Opt. Phys*., Vol. 37, pp. 247-281

Kolts, J. H.; Brashears, H. C. & Setser, D. W. (1977). Redetermination of $N_2(C)$ and $N_2(B)$ branching ratio from the Ar($^3P_{0,2}$) + N_2 reaction. *J. Chem. Phys*., Vol. 67, pp. 2931-2933

Kolts, J. H. & Setser, D. W. (1978). Decay rates of Ar(4s,$^3P_2$), Ar(4s',$^3P_0$), Kr(5s,$^3P_2$), and Xe(6s,$^3P_2$) atoms in argon. *J. Chem. Phys*., Vol. 68, pp. 4848-4859

Kovacs, T.; Blitz, M. A. & Seakins, P. W. (2010). H-atom yields from the photolysis of acetylene and from the reaction of C_2H with H_2, C_2H_2, and C_2H_4. *J. Phys. Chem. A*, Vol. 114, pp. 4735-4741

Laux, C. O. & Kruger, C. H. (1992). Arrays of radiative transition probabilities for the N_2 first and second positive, no beta and gamma, N_2^+ first negative, and O_2 Schumann-Runge band systems. *J. Quant. Spectrosc. Radiant. Transfer*, Vol. 48, pp. 9-24

Legrand, J. C.; Diamy, A. M.; Hrach, R. & Hrachová, V. (2001). *Advances in Plasma Physics Research*, Vol. 1, ed Boriotti, S. & Dennis, D. (New York: Nova) pp. 10-19

Leutner, H. W. & Stokes, C. S. (1961). Producing acetylene in a plasma jet. *Industrial and Engineering Chemistry*, Vol. 53, pp. 341-342

Luque, J. & Crosley, D. R. (1999). "*LIFBASE: Database and spectral simulation (version 1.5)*", *SRI International Report MP 99-009*

Möller, W. (1993). Advances in plasma physics research. *Appl. Phys*. A, Vol. 56, pp. 527-546

Murugavel, R. & Pothiraja, R. (2003). Synthesis, spectral characterization and crystal structures of organophosphonic diamides: pyramidal nitrogen centers and hydrogen bonding in [PhP(O)(NH^tBu)$_2$], [PhP(O)(NHDipp)$_2$](Dipp = 2,6-^{i}Pr$_2$C$_6$H$_3$) and [^{t}BuP(O)(NH^iPr)$_2$]. *New J. Chem*., Vol. 27, pp. 968-974

Murugavel, R.; Pothiraja, R.; Gogoi, N.; Clérac, R.; Lecren, L.; Butcher, R. J. & Nethaji, M. (2007). Synthesis, magnetic behaviour, and X-ray structures of dinuclear copper

complexes with multiple bridges. Efficient and selective catalysts for polymerization of 2,6-dimethylphenol. *Dalton Trans.*, pp. 2405-2410

Nguyen, T. D. & Sadeghi, N. (1983). Rotational and vibrational distributions of $N_2(C\ ^3\Pi_u)$ excited by state-selected $Ar(^3P_2)$ and $Ar(^3P_0)$ metastable atoms. *Chem. Phys.*, Vol. 79, pp. 41-55

Pancheshnyi, S. V.; Starikovskaia, S. M. & Starikovskii, A. Y. (2000). Collisional deactivation of $N_2(C^3\Pi_u, v= 0,1,2,3)$ states by N_2, O_2, H_2 and H_2O molecules. *Chem. Phys.*, Vol. 262, pp. 349-357

Pastol, A. & Catherine, Y. (1990). Optical emission spectroscopy for diagnostic and monitoring of CH_4 plasmas used for a-C:H deposition. *J. Phys. D: Appl. Phys.*, Vol. 23, pp. 799-805

Pitts, W. M.; Pasternack, L. & McDonald, J. R. (1982). Temperature dependence of the $C_2(X^1\Sigma_g^+)$ reaction with H_2 and CH_4 and $C_2(X^1\Sigma_g^+$ and a $^3\Pi_u$ equilibrated states) with O_2. *Chem. Phys.*, Vol. 68, pp. 417-422

Polak-Dingels, P. & Djeu, N. (1983). Determination of $N_2(B^3\Pi_g)$ and $N_2(C^3\Pi_u)$ vibrational temperatures in *e*-beam pumped Ar-N_2 and He-Ar-N_2 mixtures. *J. Appl. Phys.*, Vol. 54, pp. 6818-6821

Pothiraja, R.; Milanov, A. P.; Barreca, D.; Gasparotto, A.; Becker, H. W.; Winter, M.; Fischer, R. A. & Devi, A. (2009). Hafnium carbamates and ureates: new class of precursors for low-temperature growth of HfO_2 thin films. *Chem. Commun.*, pp. 1978-1980

Pothiraja, R.; Milanov, A.; Parala, H.; Winter, M.; Fischer, R. A. & Devi, A. (2009). Monomeric malonate precursors for the MOCVD of HfO_2 and ZrO_2 thin films. *Dalton Trans.*, pp. 654-663

Pothiraja, R.; Bibinov, N. & Awakowicz, P. (2010). Pulsed corona plasma source characterization for film deposition on the inner surface of tubes. *J. Phys. D: Appl. Phys.*, Vol. 43, p. 495201 (10pp)

Pothiraja, R.; Bibinov, N. & Awakowicz, P. (2011). Amorphous carbon film deposition on the inner surface of tubes using atmospheric pressure pulsed filamentary plasma source. *J. Phys. D: Appl. Phys.*, Vol. 44, p. 355206 (10pp)

Prat, R.; Koh, Y. J.; Babukutty, Y.; Kogoma, M.; Okazaki, S. & Kodama, M. (2000). Polymer deposition using atmospheric pressure plasma glow (APG) discharge. *Polymer*, Vol. 41, pp. 7355-7360

Rajasekaran, P.; Mertmann, P.; Bibinov, N.; Wandke, D.; Viöl, W. & Awakowicz, P. (2009). DBD plasma source operated in single-filamentary mode for therapeutic use in dermatology. *J. Phys. D: Appl. Phys.*, Vol. 42, p. 225201 (10pp)

Sadeghi, N. & Setser, D. W. (1981). Primary $N_2(B)$ vibrational distributions from excitation-transfer reactions between $Kr(^3P_2)$ or $Xe(^3P_2)$ atoms and N_2. *Chem. Phys. Lett.*, Vol. 82, pp. 44-50

Sadeghi, N.; Cheaib, M. & Setser, D. W. (1989). Comparison of the $Ar(^3P_2)$ and $Ar(^3P_0)$ reactions with chlorine and fluorine containing molecules: Propensity for ion–core conservation. *J. Chem. Phys.*, Vol. 90, pp. 219-231

Shul, R. J.; Passarella, R.; Yang, X. L.; Keesee, R. G. & Castleman, J. A. W. (1987). Studies of the energy dependence of reactions of Ar^+ and Ar_2^+ with CH_4 and CS_2. *J. Chem. Phys.*, Vol. 87, pp. 1630-1636

Shiu, Y. J. & Biondi, M. A. (1978). Dissociative recombination in argon: Dependence of the total rate coefficient and excited-state production on electron temperature. *Phys. Rev.* A, Vol. 17, pp. 868-872

Sieck, L. W. & Lias, S. G. (1976). Rate coefficients for ion-molecule reactions I. Ions containing C and H. *J. Phys. Chem. Ref. Data*, Vol. 5, pp. 1123-1146

Stefanović, I.; Bibinov, N. K.; Deryugin, A. A.; Vinogradov, I. P.; Napartovich, A. P. & Wiesemann, K. (2001). Kinetics of ozone and nitric oxides in dielectric barrier discharges in O_2/NO_x and $N_2/O_2/NO_x$ mixtures. *Plasma Sources Sci. Technol.*, Vol. 10, pp. 406-416

Tellinghuisen, J. B.; Winkler, C. A.; Freeman, C. G.; McEwan, M. J. & Phillips, L. F. (1972). Quenching rates of N_2^+, N_2O^+, and CO_2^+ emission bands excited by 58.4 nm irradiation of N_2, N_2O, and CO_2. *J. Chem. Soc., Faraday Trans. 2*, Vol. 68, pp. 833-838

Touzeau, M. & Pagnon, D. (1978). Vibrational excitation of $N_2(C)$ and $N_2(B)$ by metastable argon atoms and the determination of the branching ratio. *Chem. Phys. Lett.*, Vol. 53, pp. 355-360

Tsang, W. & Hampson, R. F. (1986). Chemical kinetic data base for combustion chemistry. Part I. Methane and related compounds. *J. Phys. Chem. Ref. Data*, Vol. 15, pp. 1087-1279

Velazco, J. E.; Kolts, J. H. & Setser, D. W. (1978). Rate constants and quenching mechanisms for the metastable states of argon, krypton, and xenon. *J. Chem Phys.*, Vol. 69, pp. 4357-4373

Veldhuizen, E. M. v.; Rutgers, W. R. & Ebert, U. (2002). *Int. Symp. HAKONE VIII*, Pühajärve, Estonia, pp. 33-37

Veldhuizen, E. M. v.; Nijdam, S.; Luque, A.; Brau, F. & Ebert, U. (2009). 3D properties of pulsed corona streamers. *Eur. Phys. J. Appl. Phys.*, Vol. 47, p. 22811 (5pp)

Wang, L.; Huang, L.; Wang, Y.; Xie, Z. & Wang, X. (2008). Duplex diamond-like carbon film fabricated on 2Cr13 martensite stainless steel using inner surface ion implantation and deposition. *Surf. Coat. Technol.*, Vol. 202, pp. 3391-3395

Yao, S. L.; Suzuki, E.; Meng, N. & Nakayama, A. (2002). A high-efficiency reactor for the pulsed plasma conversion of methane. *Plasma Chemistry and Plasma Processing*, Vol. 22, pp. 225-237

Yoshiki, H.; Abe, K. & Mitsui, T. (2006). SiO_2 thin film deposition on the inner surface of a poly(tetra-fluoroethylene) narrow tube by atmospheric pressure glow microplasma. *Thin Solid Films*, Vol. 515, pp. 1394-1399

Yoshiki, H. & Mitsui, T. (2008).TiO_2 thin film coating on a capillary inner surface using atmospheric-pressure microplasma. *Surf. Coat. Technol.*, Vol. 202, pp. 5266-5270

Yoshiki, H. & Saito, T. (2008). Preparation of TiO_2 thin films on the inner surface of a quartz tube using atmospheric-pressure microplasma. *J. Vac. Sci. Technol.* A, Vol. 26, 338-343

Zhiglinski A G 1994 *Handbook of Rate Constants of Process of Atoms, Electrons and Photons* (St. Petersburg: St. Petersburg university press) (in Russian)

IntechOpen

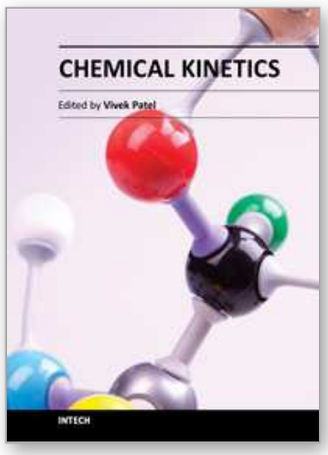

Chemical Kinetics

Edited by Dr Vivek Patel

ISBN 978-953-51-0132-1

Hard cover, 344 pages

Publisher InTech

Published online 29, February, 2012

Published in print edition February, 2012

Chemical Kinetics relates to the rates of chemical reactions and factors such as concentration and temperature, which affects the rates of chemical reactions. Such studies are important in providing essential evidence as to the mechanisms of chemical processes. The book is designed to help the reader, particularly students and researchers of physical science, understand the chemical kinetics mechanics and chemical reactions. The selection of topics addressed and the examples, tables and graphs used to illustrate them are governed, to a large extent, by the fact that this book is aimed primarily at physical science (mainly chemistry) technologists. Undoubtedly, this book contains "must read" materials for students, engineers, and researchers working in the chemistry and chemical kinetics area. This book provides valuable insight into the mechanisms and chemical reactions. It is written in concise, self-explanatory and informative manner by a world class scientists in the field.

InTech Europe
University Campus STeP Ri
Slavka Krautzeka 83/A
51000 Rijeka, Croatia
Phone: +385 (51) 770 447
Fax: +385 (51) 686 166
www.intechopen.com

InTech China
Unit 405, Office Block, Hotel Equatorial Shanghai
No.65, Yan An Road (West), Shanghai, 200040, China
中国上海市延安西路65号上海国际贵都大饭店办公楼405单元
Phone: +86-21-62489820
Fax: +86-21-62489821

IntechOpen